MISSOURI S&T

Missouri University of Science and Technology

Scholars' Mine

Electrical and Computer Engineering Faculty Research & Creative Works

Electrical and Computer Engineering

01 Aug 2002

Application of Higher-Order FEM Elements to the Analysis of Microstrip Structures

H. Wang

C. L. Guo

Todd H. Hubing
Missouri University of Science and Technology

James L. Drewniak
Missouri University of Science and Technology, drewniak@mst.edu

et. al. For a complete list of authors, see *https://scholarsmine.mst.edu/ele_comeng_facwork/895*

Follow this and additional works at: https://scholarsmine.mst.edu/ele_comeng_facwork

Part of the Electrical and Computer Engineering Commons

Recommended Citation

Application of Higher-Order FEM Elements to the Analysis of Microstrip Structures

H. Wang, C.L.Guo, T. H. Hubing, J. L. Drewniak, T. P. Van Doren, R. E. DuBroff

Electromagnetic Compatibility Laboratory
Department of Electrical and Computer Engineering
University of Missouri-Rolla
Rolla, MO 65409
haoh@ece.umr.edu

Abstract

Microstrip structures, formed by metal traces printed on a dielectric substrate above a reference plane, are frequently the object of electromagnetic modeling. In this paper, hybrid FEM/MoM formulations employing conventional Whitney elements and newly developed linear-tangent/linear-normal (LT/LN) tangential vector finite elements (TVFEs) are applied to the analysis of microstrip structures with thin traces. This paper shows that the variation of the electric field below the trace is a significant issue to be addressed in microstrip structure modeling. Different mesh methods are investigated and the advantages of the LT/LN TVFEs are discussed.

INTRODUCTION

Microstrip structures, formed by metal traces printed on a dielectric substrate above a reference plane, are common in printed circuit boards and are frequently the object of electromagnetic modeling. Many techniques have been employed to analyze microstrip structures including circuit and transmission line models as well as full-wave techniques including FDTD, FDFD, MOM, FEM, TLM, PEEC and others.

Hybrid FEM/MoM methods employ a finite element method to model the geometrically complex regions of a structure and an integral equation method to model large simple structures and to bound the region being modeled with FEM [1]. When the hybrid FEM/MoM method is used to model a microstrip structure, the details of the structure are modeled by FEM, and MoM is used to provide an accurate radiation boundary condition to terminate the FEM mesh. In the FEM part, the lowest order tangential vector finite elements (TVFEs) have generally been used as basis functions. These elements are commonly referred as Whitney Elements. Because the functions do not impose normal component continuity between tetrahedral elements, they produce no spurious modes. However, these elements limit the accuracy of the finite element solution since they only provide a constant tangential field value along element edges and a linear field variation inside the element (CT/LN) [2]. Therefore, when electric fields in a certain area fluctuate very quickly, a large number of small tetrahedra has to be employed to achieve a reasonable accuracy.

For a microstrip structure modeled using a finite element technique with Whitney Elements, thinner traces require many more elements since the aspect ratios of the tetrahedral elements must be controlled. The requirement to keep aspect ratios low forces the modeler to use a relatively coarse mesh between the trace and ground plane when modeling microstrip geometries. Thus, it is not uncommon to model the space between the trace and the plane with a single layer of elements. This approach generally yields good results when the impedance of the trace is low, i.e., wide traces. However, when the impedance of the circuit being modeled is high, the results presented here indicate that a single layer of elements may not be adequate.

Higher order hierarchical TVFEs are applied in this paper to model microstrip structures with a thin trace. These elements have a linear tangential value along each element edge and a linear field variation inside the element (LT/LN). The elements employed are referred to as "hierarchical" because the lowest order Whitney basis functions are a subset of the higher order basis functions [3].

In this paper, a hybrid FEM/MoM formulation employing LT/LN TVFEs is developed and applied to microstrip structures with thin traces. The next section introduces the hybrid FEM/MoM formulation with LT/LN TVFEs. Only the FEM part is presented here. The MoM part and hybridization of FEM and MoM can be found in [4]. The following section uses the hybrid FEM/MoM based on CT/LN and LT/LN TVFEs to analyze a typical microstrip structure with a thin trace.

FORMULATION

In the hybrid FEM/MoM, FEM can be used to analyze the interior equivalent part by solving the weak form of the vector wave equation as follows:

$$\int_V \left[\left(\frac{\nabla \times \mathbf{E(r)}}{j\omega\mu_0\mu_r} \right) \bullet (\nabla \times \mathbf{w(r)}) + j\omega\varepsilon_0\varepsilon_r\mathbf{E(r)} \bullet \mathbf{w(r)} \right] dV$$

$$= \int_S (\hat{n} \times \mathbf{H(r)}) \bullet \mathbf{w(r)}\, dS - \int_V \mathbf{J}^{int}(\mathbf{r}) \bullet \mathbf{w(r)}\, dV \qquad (1)$$

where S is the surface enclosing volume V, $\mathbf{w(r)}$ is the weighting function, and $\mathbf{J}^{int}$ is an impressed source [4]. Equation (1) shows that efficient finite-element analysis of

electromagnetic fields in 3-D regions requires computation of two element matrices. These two matrices are,

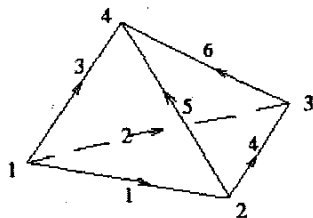$$E_{ij} = \int_V \nabla \times \mathbf{w}_i \bullet \nabla \times \mathbf{w}_j \, dV \qquad (2)$$

and

$$F_{ij} = \int_V \mathbf{w}_i \bullet \mathbf{w}_j \, dV \qquad (3)$$

where $\mathbf{w}_i$ represents the ith vector basis function and V indicates integration over one tetrahedron. The six edges of a tetrahedron are numbered as indicated in Figure 1.

Table 1. Node and edge numbering scheme of a tetrahedron

Edge#	Node 1	Node 2
1	1	2
2	1	3
3	1	4
4	2	3
5	2	4
6	3	4

**Figure 1. Edge and face definition of a tetrahedron**

The linear-tangential, linear-normal (LT/LN) basis functions associated with edge i are

$$\mathbf{w}_i^{e1} = l_i (L_{i1} \nabla L_{i2} - L_{i2} \nabla L_{i1}) \qquad i = 1, \cdots, 6 \qquad (4)$$

and

$$\mathbf{w}_i^{e2} = l_i (L_{i1} \nabla L_{i2} + L_{i2} \nabla L_{i1}) \qquad i = 1, \cdots, 6 \qquad (5)$$

where "$e1$" represents the first type of edge basis function, and "$e2$" represents the second type of edge basis function. L_i is the area coordinate associated with the node i. It is unity at node i and decays in a linear fashion to zero at the other three nodes of the cell. l_i is the length of edge i.

Figure 2 shows vector plots of these two edge-based functions in a face of a tetrahedron.
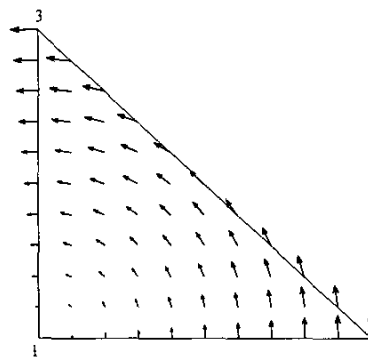
(a)
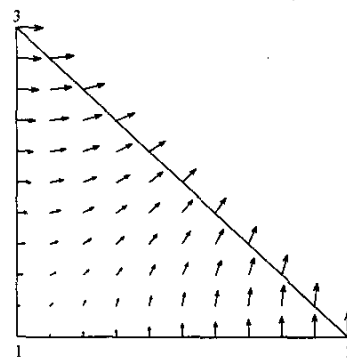
(b)

Figure 2. Plot of the basis functions. (a) $\mathbf{w}_i^{e1}$, (b) $\mathbf{w}_i^{e2}$

Using these basis functions, the electric field $\mathbf{E}$ in the interior region can be expanded as the sum of two terms

$$\mathbf{E}(r) = \sum_{k=1}^{N_e} (E_k^{e1} \mathbf{w}_k^{e1} + E_k^{e2} \mathbf{w}_k^{e2}) \cdot \qquad (6)$$

The basis function $\mathbf{w}_k$ has the following properties:

$$\mathbf{e}_k \bullet \mathbf{w}_k^{e1} = l_k \frac{L_{k1} + L_{k2}}{l_k} = L_{k1} + L_{k2} = 1 \qquad (7)$$

$$\mathbf{e}_k \bullet \mathbf{w}_k^{e2} = l_k \frac{L_{k1} - L_{k2}}{l_k} = L_{k1} - L_{k2} \qquad (8)$$

where $\mathbf{e}_k$ is a unit edge vector corresponding to the kth edge. Hence, the terms associated with "e1" elements can be considered to be the main terms, which describe fields along tetrahedron edges roughly, while the terms associated with "e2" elements can be considered to be the adjustment terms that describe the field's linear variation along the tetrahedron edges. Since CT/LN functions have one unknown per edge, they generate 6×6 local matrices. LT/LN functions have two unknowns per edge, and they generate 12×12 local matrices. Applying the LT/LN basis

functions to discretize Equation (1), a global FEM matrix can be constructed as follows,

$$\begin{bmatrix} A_{ii}^{e1e1} & A_{id}^{e1e1} & A_{ii}^{e1e2} \\ A_{di}^{e1e1} & A_{dd}^{e1e1} & A_{di}^{e1e2} \\ A_{ii}^{e2e1} & A_{id}^{e2e1} & A_{ii}^{e2e2} \end{bmatrix} \begin{bmatrix} E_i^{e1} \\ E_d^{e1} \\ E_i^{e2} \end{bmatrix} = \begin{bmatrix} 0 & 0 \\ 0 & B_{dS} \end{bmatrix} \begin{bmatrix} 0 \\ J_S \end{bmatrix} + \begin{bmatrix} g^{int} \end{bmatrix}$$
(9)

The unknown coefficients $[E_n]$ are partitioned into three types according to their corresponding basis functions and edge functions. The three categories are interior edges of "$e1$" type, which are denoted by the subscript i; dielectric boundary edges of "$e1$" type, which are denoted by the subscript d; and interior edges of "$e2$" type, which are also denoted by the subscript i. E_k^{e2} is set equal to zero on the MoM boundary to enforce the continuity of the tangential electric fields. Thus, the MoM part (employing linear basis functions) can be left unchanged during the whole process. $[JS]$ is a set of unknown complex scalar coefficients for the surface electric current densities on the FEM and MoM boundary S. $[g^{int}]$ is the source term, representing sources located within the FEM region. The elements of $[A]$, $[B_{dS}]$, and $[g^{int}]$ are given by,

$$A_{mn} = \int_V \left[\frac{(\nabla \times w_n(r)) \bullet (\nabla \times w_m(r))}{j \omega \mu_0 \mu_r} + j \omega \varepsilon_o \varepsilon_r w_n(r) \bullet w_m(r) \right] dV$$
(10)

$$B_{mn} = \int_{S_d} f_n(r) \bullet w_m(r) \, dS$$
(11)

$$g_m^{int} = -\int_V \left[J^{int} + \frac{1}{j \omega \mu_0 \mu_r} (\nabla \times M^{int}) \right] \bullet w_m(r) \, dV$$
(12)

where $f_n(r)$ is the surface basis function.

$$\begin{bmatrix} A_{ii}^{e1e1} & A_{id}^{e1e1} & A_{ii}^{e1e2} \\ A_{di}^{e1e1} & A_{dd}^{e1e1} - B_{dS}C^{-1}D & A_{di}^{e1e2} \\ A_{ii}^{e2e1} & A_{id}^{e2e1} & A_{ii}^{e2e2} \end{bmatrix} \begin{bmatrix} E_i^{e1} \\ E_d^{e1} \\ E_i^{e2} \end{bmatrix} = \begin{bmatrix} g_{int}^{e1} \\ g_{int}^{e2} \end{bmatrix} + \begin{bmatrix} B_{dS}C^{-1}F^i \end{bmatrix}$$
(13)

Equation (13) can be solved using iterative solvers.

A TYPICAL MICROSTRIP GEOMETRY

Figure 3 shows the geometry of a typical microstrip structure with a thin trace. The board is made of a dielectric material with $\varepsilon_r = 4.2$. The trace is excited by a source at one end, and is terminated by a 47-ohm resistor at the other end. The primary challenge is to model the thin trace structure.

The electric field lines around the trace are illustrated in Figure 4(a). Figure 4(b) and (c) show two possible meshes for the microstrip geometry. The coarse mesh is one layer of elements and the fine mesh is three layers of elements. In Figure 4(c), the three layers are labeled "bottom layer",

"middle layer", and "top layer" corresponding to their location in the figure. Because the electric fields vary quickly only underneath the trace, the element size on the ground plane transitions from a fine mesh underneath the trace to a coarse mesh far away from the trace. A top view of the mesh is shown in Figure 5.

The hybrid FEM/MoM is used to calculate a near field parameter (input impedance) and a far field parameter (radar cross section) for this microstrip geometry. Figure 6 illustrates the measured and calculated results for a 47-ohm termination from 200 MHz up to 1.8 GHz. For the coarse mesh with one layer of tetrahedra, the result dividing the thin trace into 20 segments along the trace is denoted "20 coarse". The results dividing the thin trace into 25, 31, 40 and 50 segments are similarly labeled. For the fine mesh with three layers of tetrahedra, the "3 layers" curve illustrates the result using the fine mesh shown in Figure 4 (c) with 40 segments along the thin trace and three layers of tetrahedra in the board thickness direction.
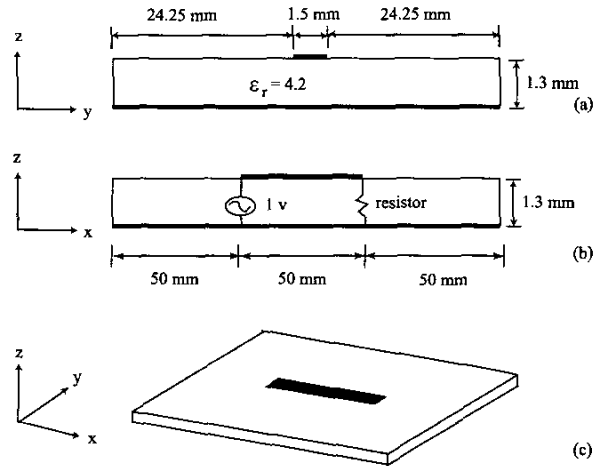

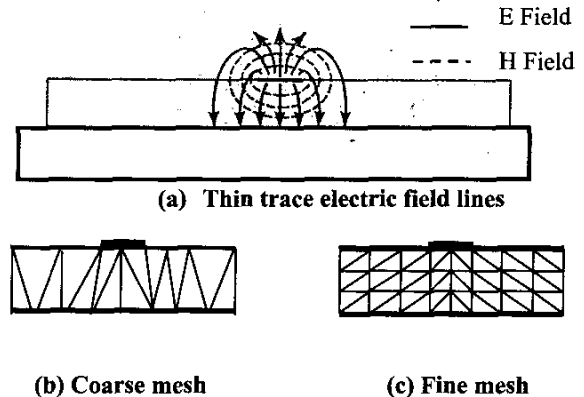Figure 3. The geometry of a microstrip structure

(a) Thin trace electric field lines

(b) Coarse mesh   (c) Fine mesh

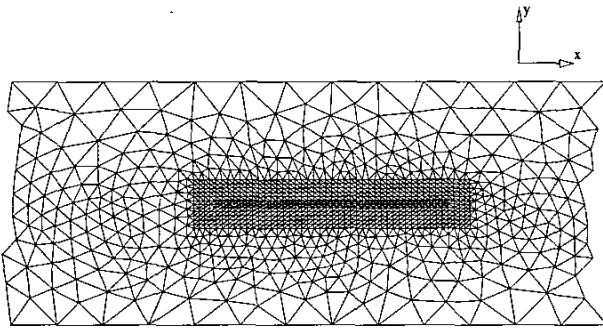Figure 4. Cross-sectional view of the electric field and FEM meshes

Figure 5. The FEM mesh in the plane of the trace

The aspect ratio of a tetrahedron is defined as the ratio of the length of the longest edge of the tetrahedron to the length of the shortest edge. Table 2 compares the maximum aspect ratios of the tetrahedra below the trace for the different meshes. From Figure 6 and Table 2, as the thin trace is divided into more segments, the aspect ratios of tetrahedra are smaller and the results with one layer of elements are closer to the measured result. However, the coarse mesh results do not converge to the measured result. Although the fine mesh with 40 segments along the trace has larger aspect ratios than the coarse meshes that have more than 30 segments, it yields a more accurate result.
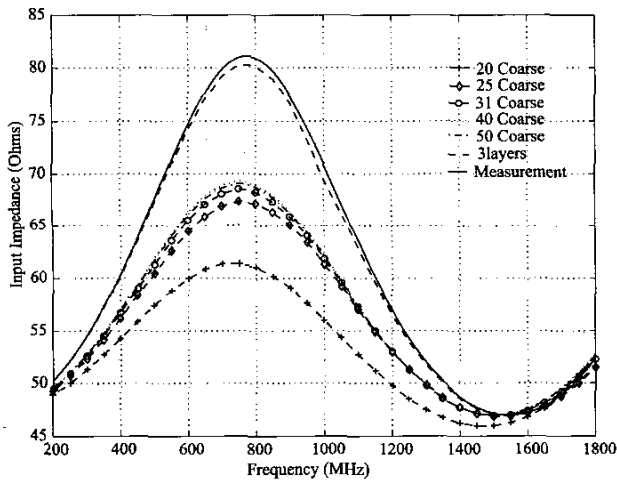

Figure 6. The measured and calculated input impedance

Figure 7 illustrates the calculated bistatic radar cross section, $\sigma = \dfrac{4\pi r^2 \, |E|^2}{a^2}$, when the angle of incidence is equal to 0 (directly above the structure). The frequency of the incident field is 800 MHz, where the difference between the coarse mesh input impedance result and that of the fine mesh was found to be the largest. The far field results have the same tendencies as the near field parameter results.

Table 2 Aspect ratios of tetrahedra comparison
(*AR = max. aspect ratio of tetrahedra)

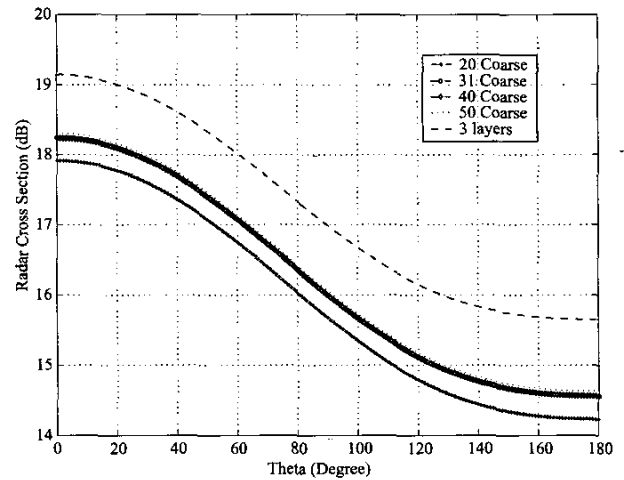| Mesh	20 coarse	25 coarse	31 coarse	40 coarse	50 coarse	3 layer
*AR	4.03	3.50	3.12	2.68	2.36	3.13

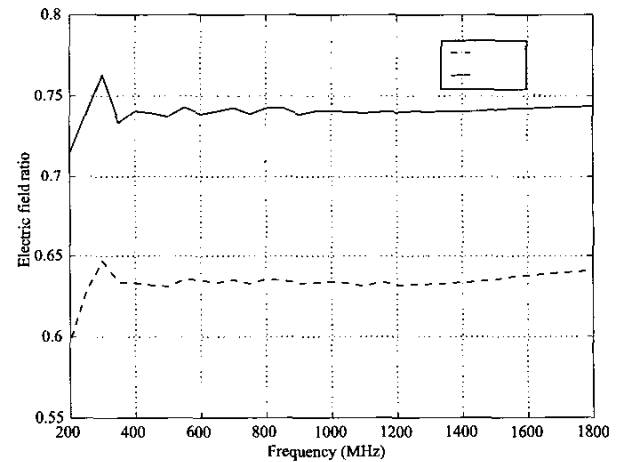

Figure 7. The calculated radar cross section

Figure 8. Comparison of the magnitudes of electric field on different layers below the trace

Figure 8 compares the magnitudes of the electric fields along the edge whose location coincides with the current source from 200 MHz to 1.8 GHz. The magnitude of the electric field in the bottom layer is denoted "Z1", and the magnitudes of the electric field in the middle layer and top layer are denoted "Z2" and "Z3". From Figure 8, the ratio of Z1 to Z3 is about 0.63 across the entire frequency range while the ratio of Z2 to Z3 is about 0.74. This means the electric field in the z direction in the top layer is much

stronger than the field in the middle and bottom layers. The *single–layer* mesh tries to represent this field with a single uniform value. This is the reason that the coarse mesh does not yield accurate results.
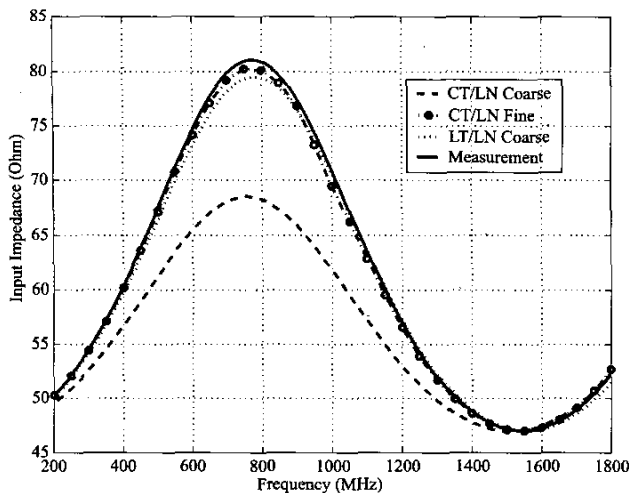

Figure 9. Input impedance of the microstrip structure using different FEM basis elements

Table 3. Comparison of computation times

FEM Part	FEM Unknowns	MoM Unknowns	FEM Matrix Non-zeros	Solver Time (sec)
CT/LN Coarse	5426	3678	27672	29.2
CT/LN Fine	9021	3678	47811	109.3
LT/LN Coarse	8451	3678	43100	68.5

Figure 9 illustrates shows the calculated input impedance for the previous geometry using the LT/LN basis functions presented in the previous section. The length of the trace was divided into 40 segments. In this figure, "coarse" denotes a mesh with one layer of tetrahedral below the trace and "Fine" denotes a mesh with 3 layers below the trace. Note that the coarse mesh yields a poor result with CT/LN elements while the LT/LN result with the coarse mesh yields an accurate result. Table 3 presents relevant parameters for the three results. For this configuration the LT/LN FEM basis functions yield provide improved accuracy with far less computer resources.

CONCLUSIONS

It is evident from this paper that the dramatic variation of the electric field below the trace is a significant issue to be addressed in microstrip structure modeling. The main parameter affecting the electric field variation is the ratio of trace width to trace height. There is a trade-off between the aspect ratio and the number of layers of tetrahedra. As illustrated in Figure 6, for microstrip structures with thin traces, it is important to have more than one layer of linear elements below the trace.

Higher order hierarchical tangential vector finite elements, LT/LN TVFEs were also employed in the hybrid FEM/MoM to analyze the microstrip structure. It was found that results calculated using the LT/LN TVFEs were significantly more accurate than the CT/LN TVFE results with a one-layer mesh. The LT/LN elements with the one-layer mesh provided results as accurate as the CT/LN elements with the three-layer mesh, but they required significantly less computational resources.

REFERENCES

[1] J. L. Volakis, T. Ozdemir, and J. Gong, "Hybrid finite-element methodologies for antennas and scattering," *IEEE Trans. Antenna and Propagation*, vol. 45, pp. 493-507, Mar. 1997.

[2] J. S. Savage and A. F. Peterson, "Higher-order vector finite elements for tetrahedral cells," IEEE Trans. Microwave Theory Tech., vol. 44, pp. 874-879, Jun. 1996.

[3] L. S. Andersen and J. L. Volakis, "Hierarchical tangential vector finite elements for tetrahedral," IEEE Microwave and Guided Wave Letters, Vol. 8, pp. 127-129, No. 3, Mar. 1998.

[4] Y. Ji and T. H. Hubing, "EMAP5: A 3D hybrid FEM/MoM code," *Appl. Computat. Electromagn. Soc. (ACES) J.*, vol. 15, pp. 1-12, Mar. 2000.